ELSEVIER

Polymer 43 (2002) 5511–5520

polymer

www.elsevier.com/locate/polymer

Generation of microcellular foams of PVDF and its blends using supercritical carbon dioxide in a continuous process

Srinivas Siripurapu[a], Yvon J. Gay[a], Joseph R. Royer[a], Joseph M. DeSimone[a,b], Richard J. Spontak[a,c]*, Saad A. Khan[a,*]

[a]*Department of Chemical Engineering, North Carolina State University, Raleigh, NC 27695-7905, USA*
[b]*Department of Chemistry, University of North Carolina at Chapel Hill, Chapel Hill, NC 27599-3290, USA*
[c]*Department of Materials Science and Engineering, North Carolina State University, Raleigh, NC 27695-7907, USA*

Received 4 March 2002; received in revised form 12 June 2002; accepted 14 June 2002

Abstract

Use of supercritical carbon dioxide ($scCO_2$) as a blowing agent to generate microcellular polymer foams (MPFs) has recently received considerable attention due to environmental concerns associated with conventional organic blowing agents. While such foams derived from amorphous thermoplastics have been previously realized, semicrystalline MPFs have not yet been produced in a continuous $scCO_2$ process. This work describes the foaming of highly crystalline poly(vinylidene fluoride) (PVDF) and its blends with amorphous polymers during extrusion. Foams composed of neat PVDF and immiscible blends of PVDF with polystyrene exhibit poor cell characteristics, whereas miscible blends of PVDF with poly(methyl methacrylate) (PMMA) yield foams possessing vastly improved morphologies. The results reported herein illustrate the effects of blend composition and $scCO_2$ solubility on PVDF/PMMA melt viscosity, which decreases markedly with increasing PMMA content and $scCO_2$ concentration. Morphological characterization of microcellular PVDF/PMMA foams reveals that the cell density increases as the PMMA fraction is increased and the foaming temperature is decreased. This study confirms that novel MPFs derived continuously from semicrystalline polymers in the presence of $scCO_2$ can be achieved through judicious polymer blending. © 2002 Published by Elsevier Science Ltd.

Keywords: Supercritical carbon dioxide; Microcellular foam; Polymer blends

1. Introduction

Microcellular polymer foams (MPFs) are porous polymers generally characterized by pore densities greater than 10^9 cells/cm^3 and cell sizes smaller than 10 μm [1]. These foams constitute an emerging class of polymeric materials that may eventually replace solid plastics in a wide range of commercial applications. Microcellular foams offer multiple advantages relative to their solid analogs, e.g. substantial material savings, decreased processing/transportation costs and improved mechanical properties. While most polymer foaming operations currently employ chlorofluorocarbons (CFCs), hydrochlorofluorocarbons (HCFCs) and volatile organic compounds (VOCs) as blowing agents, utilization of supercritical carbon dioxide ($scCO_2$) in this role provides a safer and more environmentally responsible alternative. In addition, $scCO_2$ possesses desirable physical properties, such as liquid-like densities and gas-like viscosities [2], which permit high rates of molecular diffusion in most common polymers. It, therefore, constitutes a viable alternative as a safe and efficient blowing agent for commercial foaming applications.

Microcellular foamed plastics typically exhibit high impact strength, toughness, stiffness-to-weight ratio and thermal stability, as well as a low dielectric constant and thermal conductivity, relative to their solid analogs [3]. These unique properties make MPFs ideally suited for a large number of contemporary technologies including automotive parts with high strength-to-weight ratio acoustic dampening, sporting equipment with reduced weight and high energy absorption, food packaging and insulation with reduced material costs, molecular sieves for separation processes, low dielectric insulators for microelectronic applications, surface modifiers to reduce friction, and biomedical materials for controlled drug delivery. The microcellular foaming process occurs in three steps [4]. The

* Corresponding authors. Tel.: +1-919-515-4519 (S.A. Khan) +1-919-515-4200 (R.J. Spontak); fax: +1-919-515-3465.
E-mail addresses: khan@eos.ncsu.edu (S.A. Khan), rich_spontak@ncsu.edu (R.J. Spontak).

0032-3861/01/$ - see front matter © 2002 Published by Elsevier Science Ltd.
PII: S0032-3861(02)00407-X

first step, referred to as the *saturation* step, requires saturation of a polymer melt with an inert gas under high pressure, followed by thorough mixing to form a homogeneous polymer/gas solution. The next step is the *nucleation* step, wherein a thermodynamic instability is rapidly induced so that numerous gas nuclei form uniformly throughout the polymer matrix. This is accomplished by either a pressure quench, a temperature jump or a combination of both. The final step is the *growth* step, which relates to the growth of stable nuclei and the development of desired microcellular morphology under controlled conditions.

Numerous research efforts have focused on the generation of MPFs derived from amorphous polymers, such as polystyrene (PS) [5], poly(methyl methacrylate) (PMMA) [2], polycarbonate (PC) [1] and polysulfones (PSF) [6], with $scCO_2$ in both continuous and batch processes. Reports of foaming semicrystalline polymers are, however, scarce and rely almost exclusively on batch processing. Baldwin et al. [3] have explored the feasibility of foaming amorphous polyethylene terephthalate (PET) at high CO_2 concentrations. Their results reveal that such $scCO_2$-induced crystallization severely hinders PET foaming, which, therefore, requires higher processing temperatures. While the generation of improved PET foam morphologies has been attributed to an increase in polymer matrix stiffness and a reduction in CO_2 diffusivity, the precise mechanism by which these factors affect foaming remains unclear. Doroudiani et al. [7] have shown that crystallinity is detrimental to the solubility and diffusivity of CO_2 in polymers and that, for this reason, highly crystalline polymers tend to yield non-uniform foam morphologies. Lee et al. [8] have studied the extrusion of polyethylene (PE)/PS blends in $scCO_2$ and report that high $scCO_2$ concentrations substantially reduce blend viscosity. They also found that elevated operating pressures and CO_2 levels promote small cells in PE/PS foams, but a uniform microcellular morphology is not achieved. Recent efforts by Mizumoto et al. [9] provide evidence for $scCO_2$-induced crystalline stereocomplex formation of regular PMMA, which contributed to the formation of a superior microcellular morphology during batch processing.

To the best of our knowledge, no previous studies have offered a processing strategy by which to generate, in continuous fashion, uniform microcellular morphologies derived from semicrystalline polymers. Of particular interest in the present study is the microcellular foaming of semicrystalline poly(vinylidene fluoride) (PVDF), a partially fluorinated polymer that possesses the properties of an engineering thermoplastic and a fluoropolymer. It exhibits the chemical resistance, thermal stability, dielectric properties and ultraviolet resistance of a fluoropolymer, as well as the processability of an engineering thermoplastic. These properties make PVDF a versatile polymer that is used extensively in the high-purity semiconductor market (low extraction), pulp and paper industry (chemical resistance), nuclear waste processing (radiation resistance), high-performance coatings, and the wire and cable industry (dielectric strength). Microcellular-foamed PVDF is anticipated to be highly advantageous relative to its solid counterpart due to material reduction considerations, as well as improvement in thermal and electrical insulation properties. In this work, we investigate the efficacy of foaming PVDF and its physical blends with two amorphous polymers differing in PVDF miscibility: PS and PMMA. Our continuous foaming system is detailed, as are the rheological characteristics during polymer processing with $scCO_2$ and morphological characteristics of the MPFs generated therein.

2. Experimental

2.1. Materials

The PVDF (Kynar® 740), PMMA (Plexiglas® VM-100) and PS (Lacqrene Crystal®) employed in this study were generously provided by Elf Atochem N.A. (King of Prussia, PA) in pellet form and were used without further purification. Their properties are listed in Table 1. Carbon dioxide (>99.8% pure) was obtained from National Specialty Gases (Durham, NC).

2.2. Continuous microcellular foaming system

2.2.1. Extruder configuration

A continuous extrusion-based microcellular foaming system, similar to the one developed by Park et al. [10], was employed in this study (see Fig. 1). The centerpiece of the foaming system was a 19-mm single screw extruder, manufactured by Wayne Machine and Die Co., with an extended barrel (the length to diameter ratio is 30). The extruder was divided into three sections according to feed, melt and $scCO_2$ injection. Polymer pellets were fed through a hopper into the feed section, which was continuously cooled with external water to ensure an uninterrupted polymer supply to the extruder. The melt section was outfitted with band heaters that created four sequential melt zones along the length of the barrel. A typical temperature profile for the foaming experiments conducted here is provided below the schematic of the extruder presented in

Table 1
Characteristics of the homopolymers employed in this study

Polymer	$\bar{M}_n$ [a]	$\bar{M}_w$ [a] (g/mol)	Density[b] (g/cm^3)	Melt flow index (g/10 min)
PVDF	100,000	156,000	1.78	17.5–21.5 (at 232 °C)
PS	80,000	112,000	1.05	16.0–20.0 (at 200 °C)
PMMA	70,000	107,000	1.18	14.5 (at 200 °C)

[a] Measured by gel permeation chromatography.
[b] Evaluated at 25 °C.

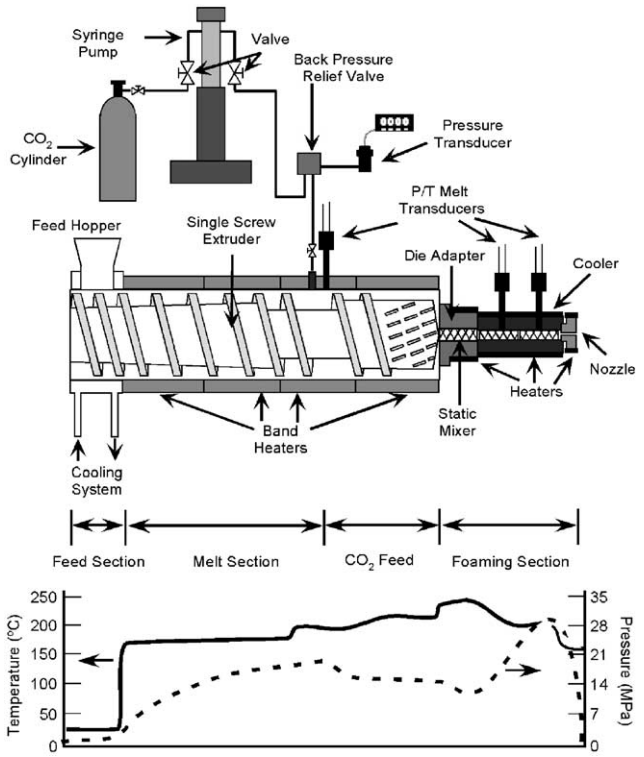

Fig. 1. Schematic illustration of a continuous extrusion-based foaming process with a typical temperature and pressure profile for foaming PVDF-containing polymer resin.

Fig. 1. According to the profile, the barrel was heated stepwise to a desired final temperature at the extruder exit. The extruder was equipped with a temperature control system accurate to within 1 °C. Blowing agents (such as $scCO_2$) were added directly to the polymer melt through an injection port located at about three-fourths the distance from the hopper to the extruder exit. A backpressure relief valve permitted accurate injection of $scCO_2$ from a syringe pump operated in constant flow mode. A detailed description of the $scCO_2$ injection system was provided elsewhere [11].

The screw design was devised specifically for microcellular foaming. Since the extruder is largely responsible for dissolving relatively large amounts of $scCO_2$ in the polymer melt, a high-pressure level was required to inhibit phase separation of the polymer/gas solution. The first part of the screw at the feed section consisted of closely spaced deep flights to ensure rapid melting of the polymer pellets. The flights became shallower as the injection port was approached to build a high-pressure zone, which served as a melt seal to avoid backflow of the blowing agent to the hopper. At the injection port, the flights were deep and spaced out, creating a low-pressure zone that facilitated $scCO_2$ injection. Beyond the port, the flights were closely spaced and shallow to increase the polymer melt pressure and promote $scCO_2$ dissolution. The final part of the screw used a Saxton mixing section to increase solution pressure and ensure polymer/gas homogeneity.

2.2.2. Foaming section design

At the exit of the extruder, microcellular foaming was achieved through the use of three separate elements: a die adapter, a cooler and a nozzle. The die adapter, equipped with a static mixer, was heated to above the extruder exit temperature to ensure complete dissolution of $scCO_2$ in the polymer melt. The cooler was also outfitted with a static mixer to reduce the system temperature in uniform and controllable fashion until the temperature was near the glass transition temperature (T_g) of the polymer/gas solution. Reduced temperature at the cooler exit was expected to enhance melt strength, prevent foam cell coalescence and increase the melt flow pressure due to an increase in polymer/gas solution viscosity. A typical pressure profile of the entire foaming process is included in Fig. 1. The nozzle served to reduce the solution pressure initiating gas nucleation in the polymer matrix. It consisted of a circular pinhole and a small channel that promotes the final growth step in the foaming process. As anticipated from the results of Behravesh et al. [5], accurate control of the experimental conditions at the cooler and nozzle allowed for excellent control of the final microcellular foam morphology. The temperatures in the die adapter and nozzle were maintained with band heaters, whereas the cooler temperature was maintained by a rope heater and a fan. The pressure drop and temperature across the cooler were measured by two Dynisco® melt transducers, and the temperatures of the two elements were maintained using individual autotune temperature control units in conjunction with type-J Omega® thermocouples.

2.3. Methods

2.3.1. Polymer foaming

In a typical experiment, the entire foaming system was heated initially to achieve a desired temperature profile. The cooler exit and nozzle temperatures were set equal to the adapter temperature. Polymer pellets were added to the extruder through the feed hopper. Polymer blends were prepared by thoroughly mixing predetermined quantities of the constituent homopolymers prior to extrusion to yield a desired composition. The extruder was operated for a reasonable period of time (ca. 15 min) at a desired screw speed to ensure steady polymer flow. Carbon dioxide was then injected into the system through the $scCO_2$ metering system. Upon reaching steady state, the extruder received a constant supply of $scCO_2$ at a fixed pressure (ca. 28–35 MPa). The melt temperature was then reduced stepwise at the cooler and nozzle elements. At lower temperatures, foaming was achieved by pressure-induced phase separation of the polymer/$scCO_2$ solution under isothermal conditions. After the bubbles nucleated, the remaining $scCO_2$ diffused into the nuclei and produced the final foam morphology, the characteristics of which reflected the operating conditions. Foamed samples were collected at different operating conditions for characterization purposes.

2.3.2. Rheological measurements

Rheological characterization of the prefoamed polymer systems containing $scCO_2$ was performed with a slit die rheometer attached to the foaming system. The design of the extrusion slit die rheometer used here was based on the original design proposed by Han and Ma [12–14] and later used by Lee et al. [15]. Its design and operating procedure were fully discussed elsewhere [11,16]. The difference between the present foaming and rheological extrusion systems was that the slit die used for rheological measurements replaced the cooler of the foaming system. The pressure drop along the length of the slit die yielded the apparent viscosity of the polymer melt under a given set of operating conditions. The slit die was maintained at constant temperature using two strip heaters (Watlow S1J10AU3) and 3 Dynisco® melt pressure and temperature transducers (TPT432A-7.5M-6/18). The homogeneity of the polymer melts containing $scCO_2$ was maintained by the downstream nozzle, which elevated the pressure of the slit die to above the bubble pressure of the polymer/CO_2 solution. Viscosity calculations were performed using standard relations for a slit die rheometer [17–19].

2.3.3. Morphological measurements

Foamed samples were dried under vacuum for 24 h at 50 °C, fractured in liquid nitrogen and examined by scanning electron microscopy (SEM) with a Hitachi S3200N variable-pressure microscope. Backscattered electron images of uncoated foams were acquired at an accelerating voltage of 21 kV and a chamber pressure of 50 Pa. Differential scanning calorimetry (DSC) of the foams was performed in a Seiko-Haake DSC220 calorimeter at a heating rate of 10 °C/min under nitrogen. Bulk densities of foamed samples were measured using Archimedes' principle, in which the measuring vessel was first calibrated with a metal sinker (since the MPFs are lighter than water). A known mass of foam was attached to the sinker and immersed in water, and the volume of the water displaced due to the immersed specimen was measured.

3. Results and discussion

3.1. Foaming PVDF

The extrusion process typically requires optimization of several operating conditions variables that influence the final foam morphology and properties. Key parameters that can be manipulated in our continuous process are (i) $scCO_2$ injection rate, (ii) residence time (screw speed), (iii) exit temperature (at cooler), (iv) foaming temperature (at nozzle), (v) pressure reduction (nozzle diameter), and (vi) depressurization rate (screw speed). Unlike conventional foaming processes performed batchwise, however, all of these process variables cannot be varied dynamically in an extrusion process. For example, fixing the screw speed establishes the residence time and the driving force for nucleation (i.e. the pressure drop for a particular nozzle). Screw speed is selected on the basis of benefiting our foaming process. A lower screw speed is preferred due to the longer residence time it permits to dissolve $scCO_2$ in the polymer melt. A very low screw speed (<10 rpm in our system) can be detrimental, as it might not promote constant flow of a high-viscosity melt. To best achieve the objective of this study, a mean screw speed of $\sim 20-25$ rpm has been chosen to ensure sufficiently long residence times and thorough mixing in the extruder barrel. All the results reported here correspond to a single nozzle diameter of about 0.5 mm, in which case only the $scCO_2$ concentration and melt and/or foaming temperature(s) can be independently varied.

Representative SEM images of PVDF foams produced at different foaming temperatures with a fixed $scCO_2$ injection rate are displayed in Figs. 2 and 3. Fig. 2a shows a PVDF foam produced at 175 °C and 2.0 wt% $scCO_2$. The corresponding enlargement (Fig. 3a) reveals that $scCO_2$-foamed PVDF possesses unacceptably poor foam structure and is not, strictly speaking, microcellular by accepted

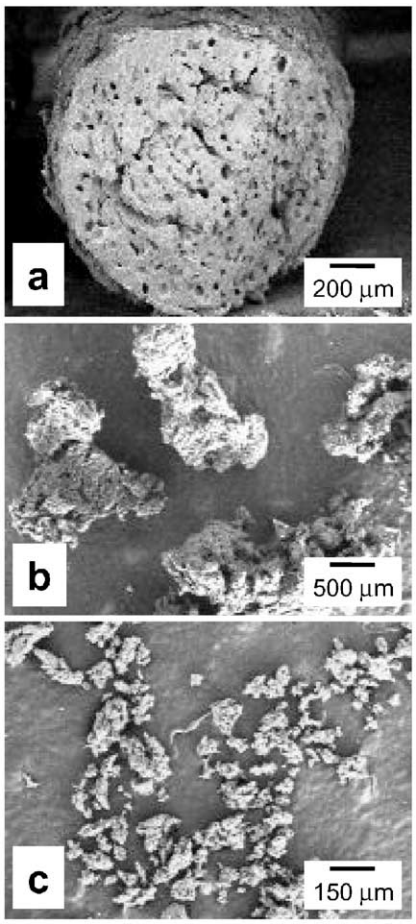

Fig. 2. SEM micrographs (imaged with backscattered electrons) of uncoated (a) PVDF foam generated at 175 °C with 2.0 wt% $scCO_2$, (b) PVDF porous powder generated at 165 °C with 2.0 wt% $scCO_2$ and (c) PVDF fine powder produced at 165 °C with 4.0 wt% $scCO_2$.

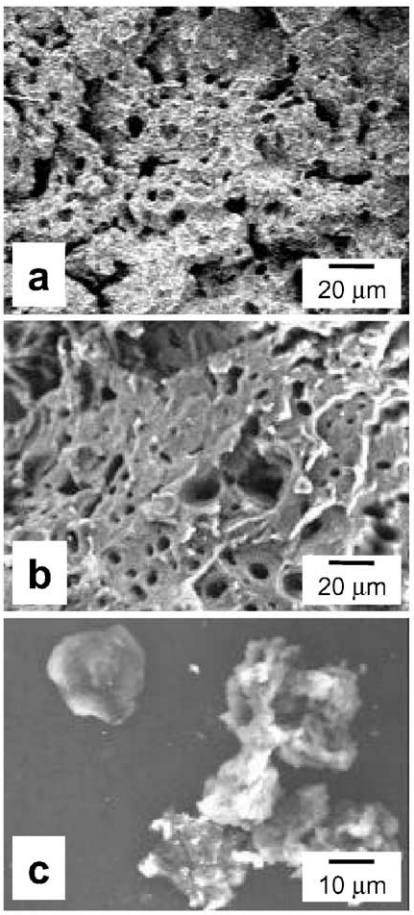

Fig. 3. SEM micrographs of uncoated (a) PVDF foam generated at 175 °C with 2.0 wt% $scCO_2$, (b) PVDF porous powder generated at 165 °C with 2.0 wt% $scCO_2$ and (c) PVDF fine powder produced at 165 °C with 4.0 wt% $scCO_2$ at higher magnification than those presented in Fig. 2.

standards. The foam exhibits a highly heterogeneous cell size distribution and a relatively low cell density. Variation in the extrusion conditions does not improve the foam morphology appreciably due to the semicrystalline nature of PVDF and its limited $scCO_2$ solubility. Although earlier studies [5] suggest that a decrease in foaming temperature to $\sim T_g$ of the polymer/CO_2 solution reduces cell coalescence and promotes high cell nucleation densities, reduction of the nozzle temperature in the present work results in the generation of PVDF powder. Micrographs of the porous PVDF powder produced in this fashion at 165 °C (under different $scCO_2$ concentrations) are displayed for comparison in Fig. 2b and c. Foaming PVDF at the low $scCO_2$ concentration (2.0 wt%) yields porous powder particles measuring 0.5–1.0 mm across. The SEM image provided in Fig. 3b confirms that the porous morphology of this powder is virtually identical to that of the foam in Fig. 3a. This morphology is characterized by the presence of fine pores varying in size and distributed in non-uniform manner. An increase in $scCO_2$ concentration substantially alters the pore morphology. Fig. 2c shows a representative micrograph of fine PVDF powder with a mean diameter of about 10–50 μm produced at 165 °C and 4.0 wt% $scCO_2$. The enlargement in Fig. 3c reveals that the powder appears to be finely ground, nonporous polymer. While this approach clearly fails to produce acceptable MPFs derived from PVDF, a detailed study regarding the feasibility of an extrusion-based $scCO_2$-assisted powder coating technology based on these results is currently underway.

Possible explanations for the unexpected behavior evident in Figs. 2 and 3 are offered below and schematically shown in Fig. 4. The T_g of PVDF is low (−40 °C), but its normal melting point (T_m) is relatively high (~170 °C). The lowest operating temperature in the extruder should be slightly higher than T_m to ensure melt flow, in which case the PVDF melt is far removed from its T_g. Foaming at these high temperatures will lead to high rates of cell coalescence and result in poor foam definition. Secondly, the solubility [20] of CO_2 in PVDF is only about 2.0 wt%. Such low solubility translates into very little gas available for foaming, thereby resulting in a small number of bubble

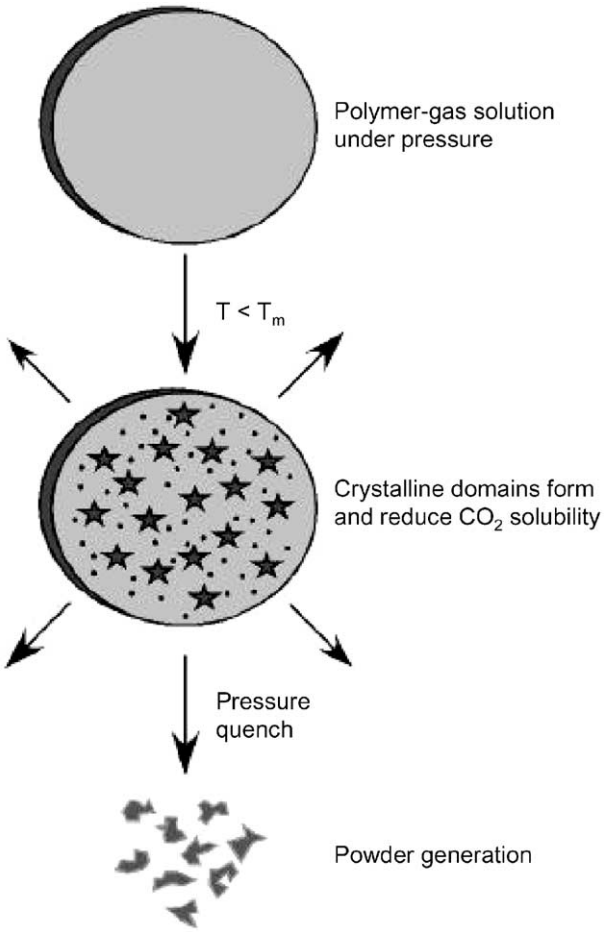

Fig. 4. Schematic diagram of the PVDF powder generation process in the presence of $scCO_2$. As the temperature of the PVDF decreases below T_m and crystals form, the solubility of CO_2 decreases, resulting in expulsion of CO_2 from the polymer. Due to the presence of impermeable crystals, the internal CO_2 pressure builds, eventually inducing fracture of the semicrystalline polymer matrix. The end result is the formation of PVDF powder.

Table 2
Thermal characteristics of PVDF subjected to $scCO_2$

Nozzle temperature (°C)	$scCO_2$ concentration (wt%)	T_g (°C)	T_m (°C)	Δh_m (J/g)
Unprocessed PVDF	–	−39.0	169.2	51.2
175	2.0	−38.9	169.4	51.8
165	2.0	−39.1	170.1	50.9
165	4.0	−40.4	168.8	49.9

Measured by differential scanning calorimetry performed at 10 °C/min.

nucleation sites. Lastly, the crystallinity of PVDF presents another obstacle, since penetrant molecules only reside within the amorphous regions of a polymer matrix. A reduction in temperature below T_m causes the PVDF to crystallize and expel the CO_2 sorbed in the melt at elevated temperatures. This mechanism may result in embrittled cell walls that would collapse upon exiting the nozzle, in which case the foam would fracture into discrete particles. An increase in $scCO_2$ concentration reduces the size of the powder insofar that fine particles no longer appear porous (see Fig. 3c). The DSC data in Table 2 compare the thermal signatures of the foamed PVDF blends with the initial polymer pellets received from the manufacturer. Unlike studies of PET, these data do not show any evidence of $scCO_2$-induced crystallization in PVDF.

3.2. Foaming PVDF blends

Physical blending is commonly employed as a means by which to modify the physical properties of macromolecular systems. Typically, polymer blending is conducted to develop low-cost materials or materials with formulation-dependent properties. Since the addition of PE to isotactic polypropylene (iPP) to form an immiscible blend in a $scCO_2$ batch process produces finer microcellular morphologies compared to foams generated from either homopolymer [7], we have elected to investigate the effect of adding PS and PMMA to PVDF as processing aids by which to produce high-quality PVDF-containing MPFs.

3.2.1. PVDF–PS blends

As most early microcellular foaming studies [21] have been successfully performed with PS, it is sensible to consider blending PVDF with PS here, although it must be remembered that the two polymers are highly incompatible. Fig. 5a is an illustrative image of a PS MPF produced with 6.0 wt% $scCO_2$ at 120 °C in our extrusion process. The foam morphology is uniformly microcellular with a cell density of about 10^{10} cells/cm^3 and a mean cell diameter of less than 10 μm. Blending PS with PVDF permits access to new processing windows in terms of lower foaming temperature and higher CO_2 uptake. Both considerations should serve to improve the overall PVDF foam morphology. Fig. 6a and b shows SEM images of foams derived from 50/50 w/w PVDF/PS blends at two different operating conditions. The

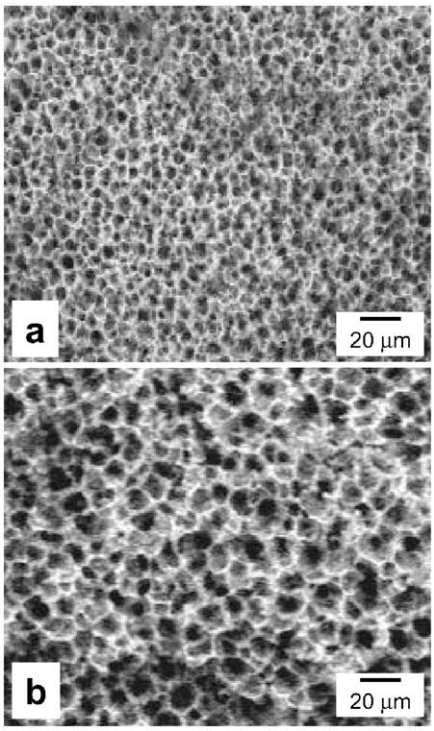

Fig. 5. Backscattered SEM micrographs of uncoated (a) PS and (b) PMMA foam generated at 120 °C with 6.0 wt% $scCO_2$.

foam presented in Fig. 6a corresponds to the blend prepared at the same conditions as the neat PVDF in Fig. 2a, whereas Fig. 6b reveals the morphology of the blend produced at 160 °C and 6.0 wt% $scCO_2$. In both cases, these foams show little improvement over those derived from neat PVDF and lack the homogeneous microcellular foam morphology achieved in neat amorphous resins. As the image in Fig. 6b

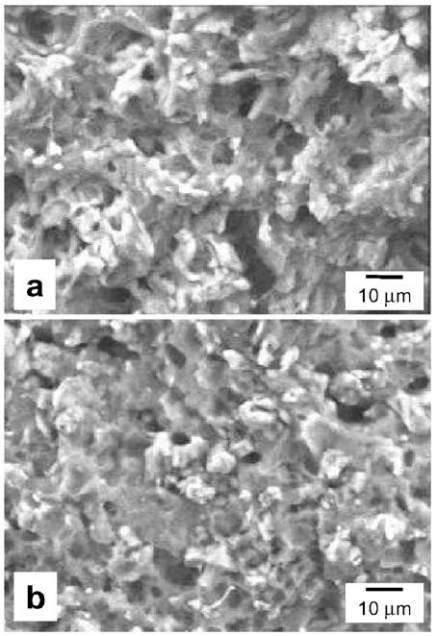

Fig. 6. Backscattered SEM images of 50/50 w/w PVDF/PS foams generated at (a) 175 °C with 2.0 wt% $scCO_2$ and (b) 160 °C with 6.0 wt% $scCO_2$.

Table 3
Thermal characteristics of MPFs derived from PVDF blends at 160 °C and 6.0 wt% $scCO_2$

Blend series	Composition (wt% PVDF)	T_g (°C)	T_m (°C)	Δh_m (J/g)	Δh_m (J/g_{PVDF})
PVDF/PS	0	104.0	–	–	–
	20	−39.0/104.0	167.8	12.6	63.0
	40	−39.0/104.0	167.6	18.9	47.3
	60	−39.0/104.6	169.3	26.5	44.2
	80	−39.0/104.1	169.2	36.7	45.9
	100	−39.0	169.1	51.0	51.0
PVDF/PMMA	0	101.0	–	–	–
	20	76.4	–	–	–
	40	49.0	–	–	–
	60	34.4	155.0	9.3	15.5
	80	−4.9	165.4	29.2	36.5
	100	−39.0	169.1	51.0	51.0

Measured by differential scanning calorimetry performed at 10 °C/min.

attests, lowering the foaming temperature and increasing the $scCO_2$ concentration does not alleviate this problem. The effect of increasing the PS content in the blends (up to 80 wt%) has also been explored. These results (not shown here) do not, however, provide any evidence for improvement. Processing a 20/80 w/w PVDF/PS blend at 160 °C and 6.0 wt% $scCO_2$, for example, does not appear to refine the foam morphology.

The thermal signatures of PVDF/PS foams over the entire blend composition range are listed in Table 3. These DSC data demonstrate that the blends are heterogeneous at all compositions. Although the heat of melting (Δh_m) of the blend decreases upon addition of amorphous PS, the degree of PVDF crystallinity in each blend can be inferred from the heat of melting of the PVDF in the blend (Δh_m expressed in J/g_{PVDF}) and does not vary markedly. Note that Δh_m of the blend is never eliminated, even in the blend with the lowest PVDF content. The presence of two discrete polymer phases during foaming strongly suggests that (i) *homogeneous* nucleation of the blowing agent occurs as expected in each phase and (ii) *heterogeneous* nucleation likewise occurs along the PVDF/PS interfaces. The extent of interfacial development is determined by the temperature, degree of $scCO_2$-induced plasticization and the degree of mixing achieved within the extruder. Foaming the polymer blend at a temperature higher than the melting point of PVDF permits considerable cell coalescence (see Fig. 6a) due to poor melt strength of the polymer, which is consequently unable to resist gas expansion. A reduction in foaming temperature results in not only greater polymer melt strength, but also higher PVDF crystallinity, the latter of which limits the availability of CO_2 gas for foaming. The presence of effectively impermeable PVDF crystals is responsible for the non-uniform foam morphology evident in Fig. 6b. These foaming results employing PVDF/PS blends are not entirely surprising, since similar morphologies have been previously reported [8] for foams based on PE/PS blends. It is interesting to note, however, that the bulk densities of the PVDF/PS foams are lower (by as much as 20–50%) than those generated from neat PVDF, despite the obvious lack of improvement in foam morphology.

3.2.2. PVDF/PMMA blends

Attempts to foam PVDF/PS blends highlight the possibility that blend miscibility may play a critical role in the generation of MPFs containing PVDF. Poly(methyl methacrylate) is another polymer that has been repeatedly shown [4] to be amenable to microcellular foaming. Fig. 5b displays a typical micrograph of an extruded MPF derived from PMMA and processed with 6.0 wt% $scCO_2$ at 120 °C, and confirms that PMMA can yield highly uniform MPFs with cell densities on the order of 10^{10} cells/cm^3 and cell diameters measuring about 10 μm across. Numerous studies [22–28] of PVDF/PMMA blends have demonstrated that these homopolymers are miscible over a reasonably broad concentration range at routine application temperatures. In fact, they exhibit lower critical solution temperature (LCST) behavior [22], which means that they tend to remain homogeneous at low temperatures and phase-separate as the temperature is increased beyond the binodal (cloud point) temperature. Such blends exhibit excellent chemical and flame resistance (due to PVDF) and reduced smoke toxicity (due to PMMA) [29]. Since PVDF is a relatively expensive polymer whereas PMMA is much less expensive, dilution of PVDF with PMMA also provides a significant economic incentive. As in the case of the PVDF/PS blends, addition of PMMA to PVDF is expected to permit foam generation at reduced temperatures and elevated $scCO_2$ concentrations.

To elucidate the roles of PMMA blending and $scCO_2$ solvation on the viscosity of PVDF, high-pressure rheological experiments have been conducted. Only a few key results are presented here to establish the effect of system (neat polymer and blend) viscosity on foam morphology. Interested readers are referred to detailed studies of PVDF/PMMA blend rheology [22,24] and $scCO_2$-induced plasticization [11,16,30–32] for more in-depth discussion. The apparent viscosity of PVDF, PMMA and PVDF/PMMA

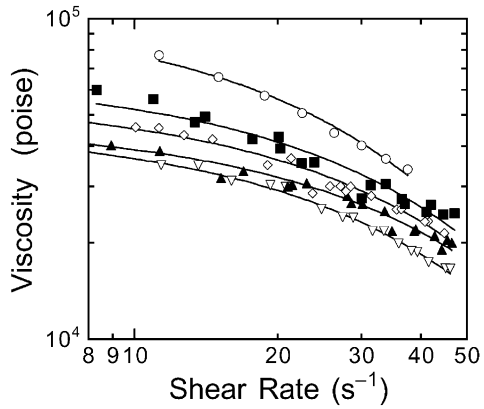

Fig. 7. Apparent melt viscosity presented as a function of shear rate at 210 °C for neat PVDF and PMMA, as well as for several PVDF/PMMA blends differing in composition (in wt% PMMA): 100 (▽), 80 (▲), 40 (◇), 20 (■) and 0 (○). Solid lines serve as guides for the eye.

blends is provided as functions of shear rate and $scCO_2$ concentration in Fig. 7. As the concentration of PMMA in the blends is increased, the viscosity expectedly decreases towards the viscosity of pure PMMA. The solid lines displayed in Fig. 7 serve as guides for the eye to identify trends and are not intended as model fits to the experimental data. Diffusion and mixing of $scCO_2$ within a polymer melt depends on the viscosity of the melt [16], in which case the lower viscosity of the blends relative to that of neat PVDF provides an indication that the blends should yield more uniform MPFs. As $scCO_2$ is added to the blends, the melt viscosity further decrease (see Fig. 8). At each blend formulation (from pure PVDF to pure PMMA) the viscosity of the system containing $scCO_2$ is significantly lower. Besides this significant viscosity reduction, addition of PMMA to PVDF increases the solubility of $scCO_2$ in the blend relative to that in neat PVDF. Rheological tests of PVDF could only be conducted at $scCO_2$ concentrations of 2.0 wt% or less. At higher concentrations, the PVDF/CO_2 mixture becomes unstable (due to phase separation) during measurement in the slit die. All the blends, including the one with 80 wt% PVDF, could be measured at concentrations of at least 4.0 wt%. This is an important consideration, since classical nucleation theory predicts [2] that higher $scCO_2$ concentration should result in smaller cell sizes.

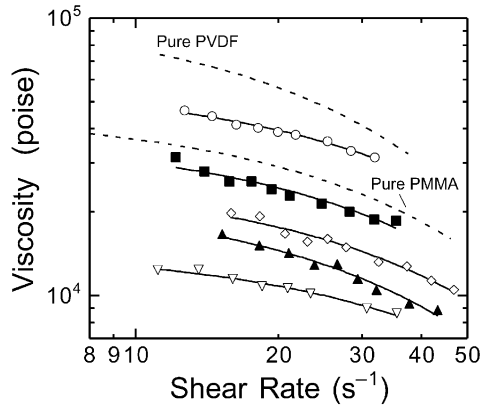

Fig. 8. Dependence of viscosity on shear rate at 210 °C for PVDF in the presence of 2.0 wt% $scCO_2$, as well as for three PVDF/PMMA blends and unblended PMMA in the presence of 4.0 wt% $scCO_2$ (in wt% PMMA): 100 (▽), 80 (▲), 50 (◇), 20 (■) and 0 (○). Solid lines serve as guides for the eye. Dashed lines representing data acquired from neat PVDF and PMMA in the absence of $scCO_2$ are included for comparison with Fig. 7.

As anticipated from the rheological measurements discussed above and confirmed by the SEM images displayed in Fig. 9, addition of PMMA to PVDF vastly improves the quality of the MPFs relative to those generated from neat PVDF. In addition to melt viscosity, the T_g of the blend constitutes an important design consideration, since it dictates the temperature at which cell coalescence ceases and the foam morphology is frozen-in. Thermal analysis of the foamed blends shown in Fig. 9 indicates that T_g of the blend increases with increasing PMMA content (see Table 3). In addition, T_m is also depressed due to PVDF dilution, yielding a narrower $T_m - T_g$ process window relative to neat PVDF. As an example, consider the 50/50 w/w PVDF/PMMA blend with $T_g = 60$ °C and $T_m = 150$ °C. Melt extrusion may be conducted at 150 °C, and foam vitrification occurs at 60 °C, thereby requiring a 90 °C temperature quench. Recall that the $T_m - T_g$ process window for neat PVDF is about 210 °C. Thus, foaming at temperatures closer to the T_g of the melt serves to reduce the degree of cell coalescence and improve the overall cell morphology. At lower PVDF concentrations (<50 wt%), the PVDF/PMMA blends are homogeneous and entirely amorphous. The effect of varying blend composition, in 20 wt% PMMA increments, on foam morphology at 160 °C and 6.0 wt% $scCO_2$ is evident in Fig. 9. As seen in Fig. 9a and b, homogeneous nucleation of miscible PVDF/PMMA blends accounts for the most uniform MPF morphologies with acceptably small cell diameters. The presence of distinct polymer phases enhances cell coalescence (Fig. 9d) and yields foam morphologies similar to that of the PVDF/PS blend (Fig. 6).

Another aspect of microcellular foaming is control over the MPF density. In the present work, the cell size distribution and, in turn, the bulk density of MPFs derived from a 40/60 w/w PVDF/PMMA blend have been systematically altered by varying the melt and foaming temperatures. Fig. 10 displays a series of SEM images of the PVDF/PMMA MPFs at different temperatures and 6.0 wt% $scCO_2$. These images clearly demonstrate that a combination of lower melt and foaming temperatures results in the best MPF morphologies, in agreement with previous findings for amorphous homopolymers. A reduction in melt temperature increases the melt strength and endows the melt with greater resistance to gas expansion in the cell growth step of the foaming process. A lower foaming temperature solidifies the skin of the foam and reduces the extent to which CO_2 diffuses from the melt to the atmosphere at the nozzle exit. Values of cell and bulk densities measured from these MPFs at different foaming temperatures are presented in Fig. 11 and confirm that these metrics can be tailored through judicious choice of foaming temperature. In fact, an increase

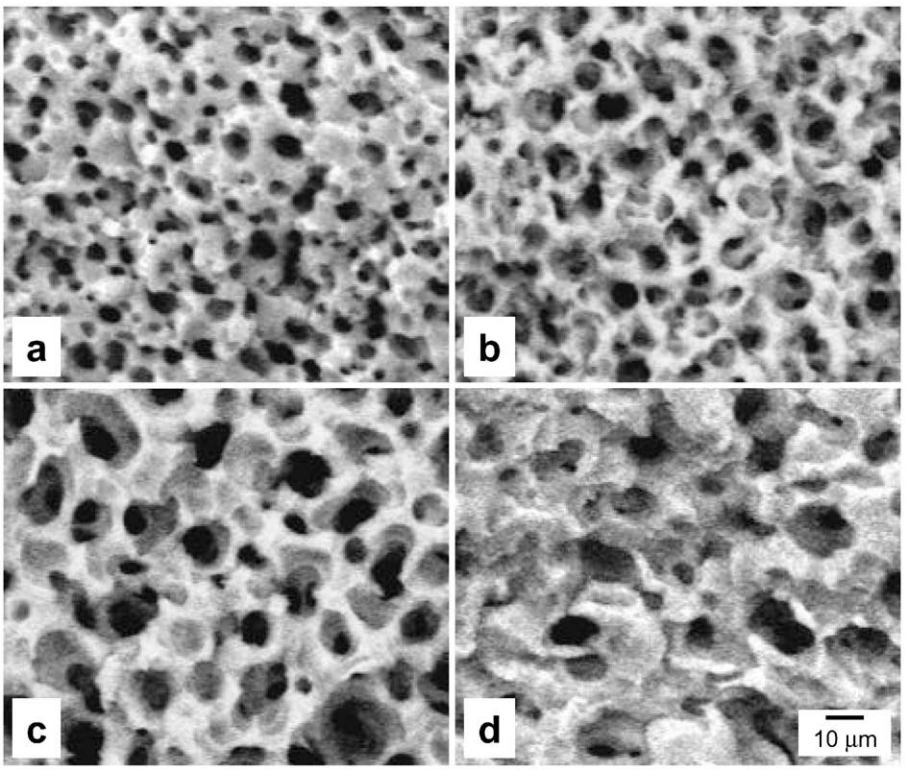

Fig. 9. Backscattered SEM images of uncoated PVDF/PMMA foams differing in composition (in wt% PMMA)—(a) 80, (b) 60, (c) 40 and (d) 20—generated at 160 °C with 6.0 wt% $scCO_2$.

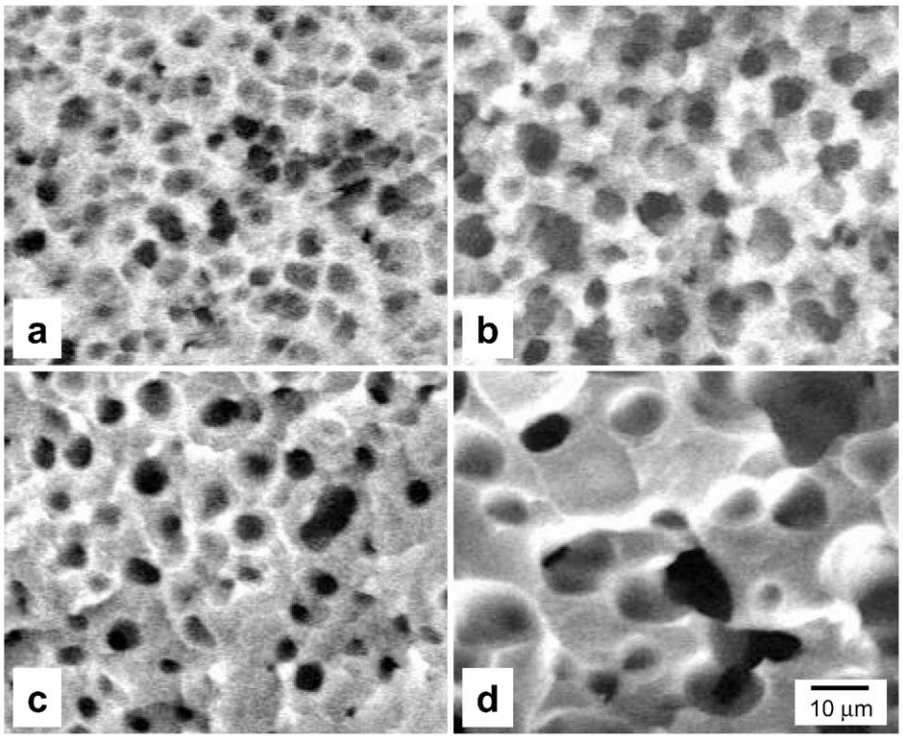

Fig. 10. Backscattered SEM images of 40/60 w/w PVDF/PMMA blends foamed at different foaming temperatures (in °C)—(a) 140, (b) 160, (c) 180 and (d) 200—with 6.0 wt% $scCO_2$.

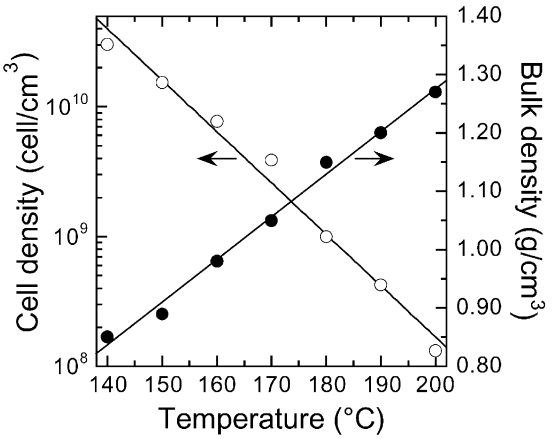

Fig. 11. Dependence of cell and bulk densities in 40/60 w/w PVDF/PMMA MPFs on foaming temperature at 6.0 wt% $scCO_2$.

of two orders of magnitude in the foam cell density is realized over the temperature range explored. Since the reduction in bulk density exceeds 70% over this range, these MPFs may be further classified as ultralight foams.

4. Conclusions

On the basis of the findings presented here, foaming PVDF/PMMA blends with $scCO_2$ affords several advantages compared to foaming neat PVDF homopolymer. Addition of PMMA to PVDF increases the solubility of $scCO_2$ from 2.0 wt% in neat PVDF to at least 6.0 wt% in PVDF/PMMA blends. Greater $scCO_2$ solubility increases the number density of bubble nucleation sites and, consequently, the cell uniformity in MPFs. It also serves to enhance the degree of plasticization and viscosity reduction. Blend homogeneity (up to about 60–70 wt% PVDF) is responsible for increasing the T_g of the blend and eliminating or, at higher PVDF concentrations, reducing the crystallinity of PVDF, which thereby alleviates the CO_2 solubility problem incurred during PVDF recrystallization. Elimination or reduction of the PVDF melting point, coupled with $scCO_2$-induced plasticization, facilitates processing the blends at lower temperatures, in which case the difference between the processing temperature and the T_g of the blend/$scCO_2$ solution is significantly reduced and provides better control over cell growth and coalescence. Blend miscibility constitutes an important issue to be considered, since blending PVDF with PS does not yield favorable MPFs due residual PVDF crystallinity, which restricts the amount of CO_2 available for foaming. The results presented here are very promising and are anticipated to establish new $scCO_2$ foaming paradigms for semicrystalline polymer resins.

Acknowledgments

The study was supported by the Kenan Center for the utilization of carbon dioxide in Manufacturing and the STC Program of the National Science Foundation under Agreement No. CHE-9876674. Y.J.G. thanks Elf Atochem N.A. for financial support.

References

[1] Kumar V, Weller JE. Polymeric foams: science and technology. Washington, DC: American Chemical Society; 1997.
[2] Goel SK, Beckman EJ. Cell Polym 1993;12:251.
[3] Baldwin DF, Park CB, Suh NP. Polym Engng Sci 1996;36:1425.
[4] Goel SK, Beckman EJ. Polym Engng Sci 1994;34:271.
[5] Behravesh AH, Park CB, Venter RD. Proceedings of ANTEC'98 1998;1958–67.
[6] Krause B, Mettinkhof R, Vegt NFAvd, Wessling M. Macromolecules 2001;34:874.
[7] Doroudiani S, Park CB, Kortschot MT. Polym Engng Sci 1998;38:1205.
[8] Lee MH, Park CB, Tzoganakis C. Polym Engng Sci 1998;38:1112.
[9] Mizumoto T, Sugimura N, Moritani M, Sato Y, Masuoka H. Macromolecules 2000;33:6757.
[10] Park CB, Suh NP. Polym Engng Sci 1996;36:34.
[11] Royer JR, Gay YJ, DeSimone JM, Khan SA. J Polym Sci, Part B: Polym Phys 2000;38:3168.
[12] Ma CY, Han CD. J Cell Plast 1982;18:361.
[13] Han CD, Ma CY. J Appl Polym Sci 1983;28:831.
[14] Han CD, Ma CY. J Appl Polym Sci 1983;28:851.
[15] Lee M, Tzoganakis C, Park CB. Polym Engng Sci 38:1112.
[16] Royer JR, DeSimone JM, Khan SA. J Polym Sci, Part B: Polym Phys 2001;39:3055.
[17] Wales JLS, denOtter JL, Janeschitz-Kriegl H. Rheol Acta 1965;4:146.
[18] Macosko CW. Rheology: principles, measurements and applications. New York: VCH; 1994.
[19] Eswaran R, Janeschitz-Kriegl H, Schijif J. Rheol Acta 1963;30:83.
[20] Lora M, Lim JS, McHugh MA. J Phys Chem B 1999;103:2818.
[21] Kumar V, Suh NP. Polym Engng Sci 1990;30:1323.
[22] Mijovic J, Luo HK, Han CD. Polym Engng Sci 1982;22:234.
[23] Chiou JS, Barlow JW, Paul DR. J Appl Polym Sci 1985;30:2633.
[24] Paul DR, Barlow JW, Bernstien RE, Wahrmund DC. Polym Engng Sci 1978;18:1225.
[25] Hirata Y, Kotaka T. Polym J 1981;13:273.
[26] Nishi T, Wang TT. Macromolecules 1975;8:909.
[27] Morra BS, Stein RS. Polym Engng Sci 1984;24:311.
[28] Douglass DC, McBrierty VJ. Macromolecules 1978;11:766.
[29] Burke DM. J Vinyl Tech 1993;15:177.
[30] Wang WV, Kramer EJ, Sachse WH. J Polym Sci, Part B: Polym Phys 1982;20:1371.
[31] Elkovitch MD, Tomasko DL, Lee LJ. Polym Engng Sci 1999;39:2075.
[32] Gerhardt LJ, Manke CW, Gulari EJ. J Polym Sci, Part B: Polym Phys 1997;35:523.